Geometry-induced pulse instability in microdesigned catalysts: The effect of boundary curvature

L. Qiao and I. G. Kevrekidis*
Department of Chemical Engineering, Princeton University, Princeton, New Jersey 08544 USA

C. Punckt and H. H. Rotermund
Fritz-Haber-Institut der MPG, Faradyweg 4-6, 14195 Berlin, Germany
(Received 23 November 2005; published 24 March 2006)

We explore the effect of boundary curvature on the instability of reactive pulses in the catalytic oxidation of CO on microdesigned Pt catalysts. Using ring-shaped domains of various radii, we find that the pulses disappear (decollate from the inert boundary) at a turning point bifurcation, and we trace this boundary in both physical and geometrical parameter space. These computations corroborate experimental observations of pulse decollation.

DOI: 10.1103/PhysRevE.73.036217 PACS number(s): 05.45.−a, 82.40.Ck, 82.40.Np

I. INTRODUCTION

Pattern formation in spatially uniform media has been studied extensively (see, e.g., the review by Cross and Hohenberg [1] and, specifically for catalytic surfaces, the recent review by Imbihl [2]). Since the pioneering photoemission electron microscopy work of Ertl and co-workers in 1990 [3], high-vacuum CO oxidation on single-crystal Pt catalysts has been a paradigm for such studies. Current research increasingly focuses on the interplay between spontaneous pattern formation and spatial medium nonuniformity, as well as with spatiotemporal variations of the medium properties. Designing the geometry of the medium at the microscopic level has been finding an increasing number of applications across disciplines in recent years (e.g., Refs. [4–7]). Examples of complex, microdesigned geometries used in the study of reacting systems include Belousov-Zhabotinsky (BZ) catalyst microprinting [8] and CO oxidation on microlithographically shaped domains on Pt catalysts [9]. The study of reactive pattern formation in random heterogeneous media is a topic of active current modeling work (e.g., Refs. [10,11]); natural heterogeneous media (such as water-in-oil microemulsions in Ref. [12]) are also being studied. Microfluidics is another field that hinges on the micrometer-scale design of geometry to control flow and transport (see, e.g., the review [13]); beyond passive geometry design, extensive developments in *active* addressing, for example in control of droplet breakup [14] or micromixing [15], have been realized. Actively and spatiotemporally altering the activity of chemically reactive media is exemplified in Ref. [16] for thermally addressed heterogeneous catalytic reactions and in Ref. [17] for photosensitive BZ media. The recent work of Ref. [18] marries microfluidic technology with the active addressing of pattern forming reactive media in a developmental biology context, using temperature fields to perturb pattern formation in drosophila embryos.

The interplay of nonlinear reaction-diffusion dynamics with the effects of boundaries has been extensively studied both in theory and in experiments; a remarkable early observation was that rotating spiral waves of a BZ reagent could be initiated close to domain boundaries with sharp corners [19]. Observations in catalytic reactions include that (a) below a certain critical domain size, the frequency of rotating waves in a small circular domain is affected by the domain size [20]; and (b) the interaction of patterns with inert or active boundaries causes the pinning, transmission, and boundary backup of spirals, and instability of pulses turning around corners [21,22]. The presence of boundaries can also give rise to new patterns that have not been observed in homogeneous reaction-diffusion systems [9].

Traveling pulses in excitable media constitute an important building block of pattern formation. They have been documented in a variety of nonlinear dynamical systems, including CO oxidation on Pt(110), arising from a localized, finite perturbation of a linearly stable steady state [23,24]. The instabilities and bifurcations of solitary traveling pulses in the CO oxidation on Pt(110) have been well studied in the one-dimensional case for a wide range of parameters [25,26]. A recent study explored the effects of anisotropic diffusion on two-dimensional pulse propagation in the thin ring limit [27]. However, the experimentally observed pulses in the catalytic CO oxidation on Pt(110) propagate on a truly two-dimensional surface and interact with boundaries and heterogeneities of finite size; a more detailed study of the boundary effects on two-dimensional pulse propagation has been missing. The use of a simplified two-variable reaction-diffusion model [28] in previous studies of pulses in CO oxidation also creates some difficulty in comparing computational results with experimental data. Derived from the full, three-variable model [29] through approximations and simplifications, the parameters in the two-variable model do not have simple, explicit physical meaning; variation of such model parameters is not easy to realize experimentally.

In this paper, we use the full, three-variable Krischer-Eiswirth-Ertl (KEE) model for CO oxidation on Pt(110) to study and analyze the behavior of traveling pulses in fully two-dimensional ring structures. In particular, we perform stability and continuation computations with respect to both *physical parameters* [such as the partial pressure of

*Also at the Program in Applied and Computational Mathematics (PACM), Princeton University, Princeton, NJ 08544, USA.

CO (P_{CO})] and *geometric parameters* such as the ring radii. The curvature of an inert boundary on which a pulse is attached plays a crucial role in affecting the pulse dynamics; the ring geometry provides an ideal setting in which to study this fundamental interaction since the (constant) curvature is prescribed and can be varied systematically when constructing the domain.

The paper is organized as follows. We begin with a brief introduction to the KEE reaction-diffusion model for catalytic CO oxidation on Pt(110) in Sec. II. Section III shows the effect of boundary curvature on the stability of two-dimensional traveling pulses in two distinct cases: for fixed geometry, the dependence of pulse stability on the partial pressure of CO is first studied; then, keeping P_{CO} constant, we study the dependence of pulse stability on the boundary curvature—both inner and outer. Representative experimental results supporting the calculation are presented in Sec. IV. We briefly summarize our results and conclude in Sec. V.

II. MODELING

We use the Krischer-Eiswirth-Ertl reaction-diffusion model for CO oxidation on Pt(110) with a surface phase transition [29]. This surface reaction follows a Langmuir-Hinshelwood mechanism:

$$\mathrm{CO} + * \leftrightharpoons \mathrm{CO}_{ads},$$

$$2* + \mathrm{O}_2 \rightarrow 2\mathrm{O}_{ads},$$

$$\mathrm{CO}_{ads} + \mathrm{O}_{ads} \rightarrow 2* + \mathrm{CO}_2\uparrow,$$

accompanied by a $1\times 2 \rightarrow 1\times 1$ phase transition of the Pt(110) surface due to CO adsorption.

The equations in this kinetic model are

$$\dot{u} = k_u s_u p_{\mathrm{CO}}\left[1 - \left(\frac{u}{u_s}\right)^3\right] - k_1 u - k_2 u v + D_u \nabla^2 u, \quad (1)$$

$$\dot{v} = k_v p_{\mathrm{O}_2}[w s_{v_1} + (1-w)s_{v_2}]\left(1 - \frac{u}{u_s} - \frac{v}{v_s}\right)^2 - k_2 u v, \quad (2)$$

$$\dot{w} = k_3(f(u) - w), \quad (3)$$

where u, v, and w denote the surface coverage of CO and O, and the surface fraction of the 1×1 phase, respectively. The adsorption rate constant for CO and O_2, k_u and k_v, respectively, are set to be constant within the temperature range considered in this paper. The rate constants k_1, k_2, and k_3 for the desorption, reaction, and surface phase transition are given by the Arrhenius formula $k_i = (k^0)_i \exp(-E_i/kT)$; T is the temperature of the single crystal. We used the parameters for Pt(110) given in Table II of Ref. [29] as follows:

$$u_s = 1, \quad v_s = 0.8, \quad s_u = 1, \quad s_{v_1} = 0.6, \quad s_{v_2} = 0.4,$$

$$k_u = 3.135 \times 10^5 \ \mathrm{s}^{-1}\ \mathrm{mbar}^{-1},$$

$$k_v = 5.858 \times 10^5 \ \mathrm{s}^{-1}\ \mathrm{mbar}^{-1},$$

$$k_i = k_i^0 \exp(-E_i/kT), \quad i = 1,2, \text{ and } 3,$$

$$k_1^0 = 2 \times 10^{16}\ \mathrm{s}^{-1}, \quad E_1 = 38\ \mathrm{kcal/mol},$$

$$k_2^0 = 3 \times 10^{16}\ \mathrm{s}^{-1}, \quad E_2 = 10\ \mathrm{kcal/mol},$$

$$k_3^0 = 10^2\ \mathrm{s}^{-1}, \quad E_3 = 7\ \mathrm{kcal/mol}.$$

We used the diffusion coefficient reported in Ref. [30]:

$$D_u = D_u^0 \exp(-E_u/kT),$$

$$D_u^0 = 10^{-4}\ \mathrm{cm}^2/\mathrm{s}, \quad E_u = 7\ \mathrm{kcal/mol}.$$

The function $f(u)$ has been fitted to experimental data to give the rate of surface phase transition as a function of u, the coverage of CO, as follows:

$$f(u) = \begin{cases} 0 & \text{for } u \leqslant 0.2, \\ \dfrac{u^3 - 1.05u^2 + 0.3u - 0.026}{-0.0135} & \text{for } 0.2 < u < 0.5, \\ 1 & \text{for } u \geqslant 0.5. \end{cases}$$

The variable v can, in principle, be adiabatically eliminated to give an activator-inhibitor-type partial differential equation (PDE) system of two equations [28].

We discretize the three model equations over a two-dimensional ring-shaped domain using the finite-element method as implemented in the package FEMLAB [31]. FEMLAB provides a dynamic simulator for the problem; we want to find stable and unstable stationary (in a traveling frame) states, perform continuation and bifurcation calculations, and compute the linearized stability of the solutions we find. We used matrix-free linear algebra algorithms to perform these computations, with the right-hand side of our equations provided on demand by FEMLAB. Newton-Krylov GMRES (see, e.g., Ref. [32]) was used for stationary state computations, coupled with pseudoarclength continuation to trace the bifurcation diagrams; the Jacobian of the discretized equations was exported from FEMLAB into a MATLAB code for this purpose. ARPACK was used within MATLAB for stability computations of the resulting generalized eigenvalue problem.

Due to the symmetry of the domain, we rewrite the system of differential equations in a frame that rotates at an angular speed ω. The model equations written in comoving frame and polar coordinates are given by

$$\dot{u} = k_u s_u p_{\mathrm{CO}}\left[1 - \left(\frac{u}{u_s}\right)^3\right] - k_1 u - k_2 u v + D_u \nabla^2 u + \omega \partial_\theta u, \quad (4)$$

$$\dot{v} = k_v p_{\mathrm{O}_2}[w s_{v_1} + (1-w)s_{v_2}]\left(1 - \frac{u}{u_s} - \frac{v}{v_s}\right)^2 - k_2 u v + \omega \partial_\theta v, \quad (5)$$

$$\dot{w} = k_3(f(u) - w) + \omega \partial_\theta w, \quad (6)$$

with no-flux boundary conditions

$$\partial u/\partial r = 0, \quad \text{at } r = r_i \text{ and } r_o,$$

where r_i and r_o are the inner and outer radius of the two-dimensional ring-shaped domain, respectively. The diffusion of CO is chosen to be isotropic for simplicity. By appending an extra pinning condition to remove rotational invariance, we can find the appropriate *corotating* speed ω as well as the steady pulse shape traveling with this speed, as steady state solutions to Eqs. (4)–(6). It is worth noting that ways to find the "right" corotating speed, even during transient evolution, have been devised using a "template based" approach [33–35].

We want to study the influence, on the stability of the traveling pulses, of the boundary curvature by varying the ring radii. The ring radii do not appear explicitly in the equations, however; they only appear in the boundary conditions. We therefore first carry out a linear transformation of coordinates, mapping the physical domain (the strip between the inner radius r_i and outer radius r_o) to a *constant* computational domain (between the fixed values ρ_i, ρ_o).

Let r, θ be the independent variables in the original polar coordinates. The diffusion term in Eq. (1) is expressed as

$$\nabla^2 u = \frac{1}{r}\frac{\partial u}{\partial r} + \frac{\partial^2 u}{\partial r^2} + \frac{1}{r^2}\frac{\partial^2 u}{\partial \theta^2}, \quad r \in [r_i, r_o], \quad \theta \in (0, 2\pi].$$

Define another set of polar coordinates (ρ, ϕ)

$$\rho = (r - r_i) \times \frac{\rho_o - \rho_i}{r_o - r_i} + \rho_i, \quad \rho \in [\rho_i, \rho_o],$$

$$\phi = \theta, \quad \phi \in (0, 2\pi],$$

and express the term of CO diffusion in the new polar coordinates (in a form convenient for FEMLAB implementation):

$$\begin{aligned}\nabla^2 u &= \frac{\sqrt{c_1 c_2}}{\rho}\frac{\partial u}{\partial \rho} + c_1\frac{\partial^2 u}{\partial \rho^2} + \frac{c_2}{\rho^2}\frac{\partial^2 u}{\partial \phi^2} \\ &= \tilde{\nabla}\cdot\left(\begin{bmatrix} c_1 & 0 \\ 0 & c_2 \end{bmatrix}\cdot\tilde{\nabla}u\right) + \begin{bmatrix} \frac{\sqrt{c_1 c_2} - c_1)}{\rho}, 0 \end{bmatrix}\cdot\tilde{\nabla}u,\end{aligned} \tag{7}$$

where

$$c_1 = \left(\frac{\rho_o - \rho_i}{r_o - r_i}\right)^2, \quad c_2 = \left(\frac{\rho}{(\rho - \rho_i)\times\frac{r_o - r_i}{\rho_o - \rho_i} + r_i}\right)^2,$$

and $\tilde{\nabla}u$ is the gradient of u in the new polar coordinates. Now r_o and r_i appear explicitly in c_1 and c_2. By substituting Eq. (7) in Eq. (4), we obtain a new PDE system that can be discretized and rewritten in the comoving frame to solve for the steady pulse solutions. We plot our results in the original (r, θ) polar coordinates.

III. COMPUTATIONAL RESULTS

A. Influence of the presence of boundary

We recall some results for simple, one-dimensional solitary pulses with respect to the variation of P_{CO}, as shown in Fig. 1. The traveling speed of a *stable* solitary pulse decreases as P_{CO} increases. When P_{CO} is above some critical value (4.599×10^{-5} mbar in Fig. 1), the medium cannot support pulses any more. Checking the leading eigenvalues of the linearization of the system equations we identify the bifurcation at which the pulse is lost as a *turning point* (or saddle-node) instability: a single eigenvalue crosses zero and becomes positive as the branch of traveling pulses turns around and becomes unstable (saddle-type). For completeness, we note that toward the "other side" of the 1D bifurcation diagram, as P_{CO} is decreased, a turning point of the kinetic steady state associated with our oxygen-rich pulses is observed around $P_{CO}=4.480\times10^{-5}$ mbar; clearly, the pulses cannot exist below that P_{CO} value. Interestingly, a different family of CO-rich pulses is observed for even lower values of P_{CO} (below $P_{CO}=4.294\times10^{-5}$ mbar; see also Ref. [36]).

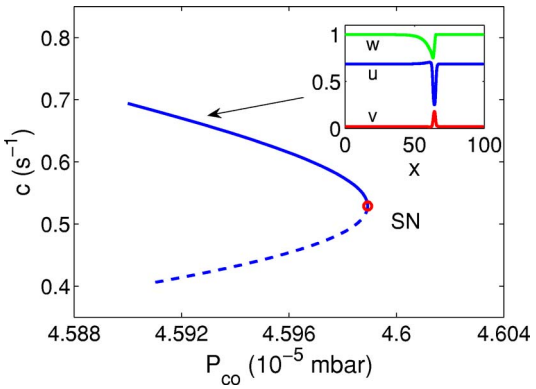

FIG. 1. (Color online) Bifurcation diagram of one-dimensional (1D) pulses with respect to the partial pressure of CO. The variable c is the propagating speed of the steady pulse (a representative one is shown in the inset). The turning point (saddle-node bifurcation) is indicated by a circle. Solid (dashed) lines denote stable (unstable) steady pulse solutions. $T=540$ K, $P_{O_2}=1.33\times10^{-4}$ mbar. The inset shows the typical shape of u, v, and w at the steady state marked by the arrow.

In a two-dimensional ring-shaped domain, the shape and stability of traveling pulses are affected by the presence of inert boundaries, as shown in Fig. 2. The insets show the oxygen coverage profile corresponding to the steady pulse at different locations along the diagram. The inner and outer radii of the ring are fixed at dimensionless values of 20 and 30, respectively (1 unit corresponds to approximately 3.8 μm). Comparing the bifurcation diagrams in Figs. 2 and 1 shows that the turning point bifurcation is still present, but now we find that the pulse loses stability before the turning point due to a Hopf bifurcation; simulations indicate that this bifurcation is subcritical. We plot the eigenmodes corresponding to the leading eigenvalues at points H and p along the diagram in Fig. 3. The leading eigenmodes at the Hopf bifurcation point H [Figs. 3(b) and 3(c)] constitute a complex pair crossing the imaginary axis and rendering the pulse unstable. The spatial structure of these eigenmodes clearly resides close to the inner boundary, suggesting that this boundary is responsible for the instability. An eigenvalue zero corresponding to the rotational invariance is also found; its eigenvector [Figs. 3(a) and 3(d)] can be obtained from the

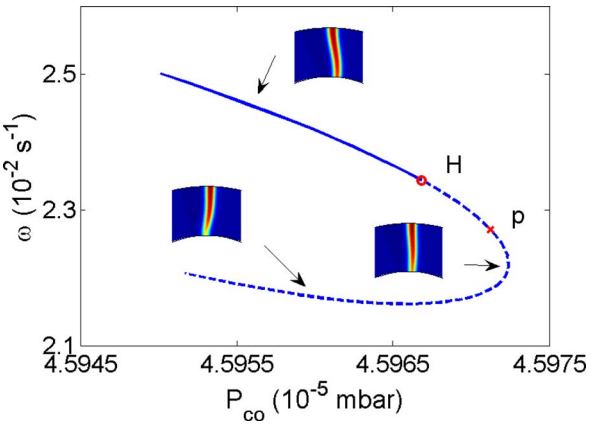

FIG. 2. (Color online) Bifurcation diagram of pulses in a two–dimensional (2D) ring showing the influence of the CO partial pressure on the angular speed (ω) of the traveling pulse at stationarity. Point H, marked with a circle, denotes a Hopf bifurcation. Solid (dashed) lines denote stable (unstable) steady pulse solutions. The insets show profiles of O coverage (for the color version, the color is scaled from blue to red according to the coverage of oxygen from low to high). The leading eigenvalues and corresponding eigenvectors at points H and p are plotted in Fig. 3 below. The inner and outer dimensionless radii of the ring are 20 and 30, respectively. $T=540$ K, $P_{O_2}=1.33\times10^{-4}$ mbar; P_{CO} is the bifurcation parameter.

pulse shape by differentiation with respect to θ. When the pulse propagates in the ring, its shape is no longer planar (see the snapshot of a pulse on the stable branch in Fig. 2); it has to curve so as to satisfy the no-flux boundary condition on both curved boundaries. The end of the pulse close to the inner boundary takes a convex shape and it is known that such a convex shape of pulses may lead to instability when the curvature grows above some critical value [24]. We will see this boundary effect on the stability of pulses more clearly below, when we present bifurcation diagrams from a direct continuation in the ring radius. After the Hopf bifurcation, the eigenvalue pair responsible for it collapses on the real axis, giving rise to two real positive eigenvalues close to point p. Figures 3(e) and 3(f) show the corresponding eigenmodes of these two real eigenvalues at point p; the absolutely smaller one of the two proceeds to cross zero at the turning point.

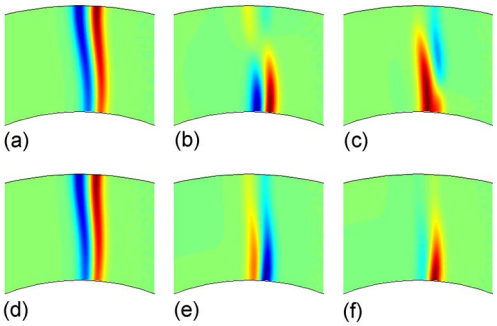

FIG. 3. (Color online) The corresponding eigenmodes of three leading eigenvalues at point H and p as in Fig. 2. (a)–(c) are eigenmodes for point H. $\lambda=$ (a) 0.0005, (b) and (c) $-0.0006\pm0.2591i$. (d)–(f) are eigenmodes for point p. $\lambda=$ (d) 0.0026, (e) 0.1172, and (f) 0.2324.

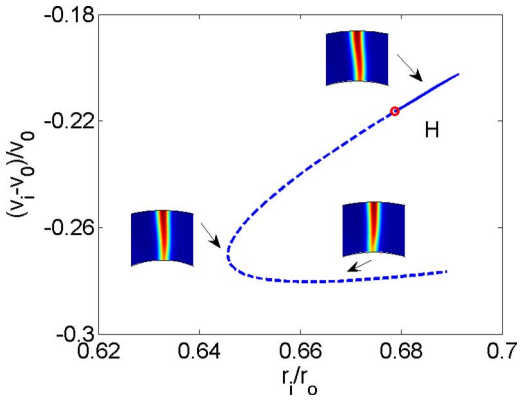

FIG. 4. (Color online) Bifurcation diagram varying the boundary curvatures while fixing ring width. v_i is the local velocity of the propagating pulse at the inner boundary. v_0 is the propagating speed of a one-dimensional pulse. The increase of boundary curvature leads to a pulse instability that is associated with a Hopf bifurcation, followed again by a turning point. $T=540$ K, $P_{O_2}=1.33\times10^{-4}$ mbar, $P_{CO}=4.597\times10^{-5}$ mbar. The ring width r_o-r_i is fixed at 8.

For the two-dimensional ring structure, the shape and stability of the pulse solutions are dictated by the choice of r_i and r_o. For more general geometries (e.g., nonconcentric boundaries) one can parametrize the geometry through the inner curvature, the outer curvature, and the distance between the boundaries. We will look at the effect of geometry taking two distinct one-parameter paths: (a) changing the radii while keeping the ring width fixed; and (b) fixing the outer boundary and varying the inner one.

B. Influence of varying the boundary curvature

Figure 4 reflects the influence of the curvature (of both boundaries) on the pulse stability with r_o-r_i held fixed. The leading eigenvalues and corresponding eigenmodes at the Hopf bifurcation point are plotted in Fig. 5. Similar to the first row of Fig. 3, the eigenmodes corresponding to the eigenvalue pair crossing the imaginary axis show some structure close to the inner boundary, but here both the Hopf and Saddle-Node (SN) bifurcation (at the turning point) are induced by the change of boundary curvature alone. The Hopf bifurcation is again subcritical (as simulations indicate).

In the limit of $r_i/r_o=1$ as $r_i\to\infty$, we should have an effectively one-dimensional planar pulse with a constant velocity v_0. As we decrease r_i, the local curvature of the pulse close to the inner boundary increases and the local shape of the pulse becomes more convex (compare the top inset in

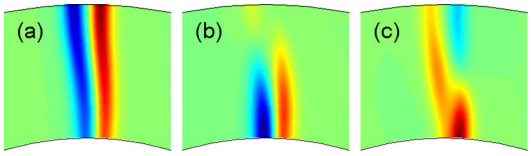

FIG. 5. (Color online) Three leading eigenvalues and corresponding eigenmodes at the Hopf bifurcation point H in Fig. 4. $\lambda=$(a) -0.0012; (b) and (c) $-0.0025\pm0.2899i$.

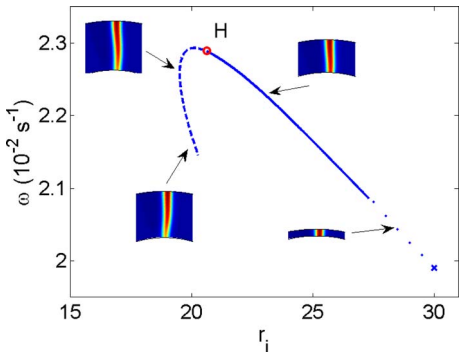

FIG. 6. (Color online) Bifurcation diagram of pulses in a 2D ring showing the influence of varying the inner ring radius r_i on the traveling pulse stability. Point H, marked with a circle, denotes a Hopf bifurcation. Solid (dashed) lines denote stable (unstable) steady pulse solutions. For r_i close to 30, steady pulse solutions are computed at discrete points. Insets show the profiles of O coverage. The dimensionless outer radius of the ring r_o is fixed at 30. $T=540$ K, $P_{O_2}=1.33\times10^{-4}$ mbar, $P_{CO}=4.597\times10^{-5}$ mbar.

Fig. 4 with a planar pulse). This is associated with a decreasing local velocity. For a stable two-dimensional pulse expanding in an infinite medium as a two-dimensional ring (with azimuthally uniform curvature), the propagating velocity (and the pulse stability) increases as the ring grows and the pulse becomes less convex [24]. There also exists a critical curvature above which no pulse solution exists. A pulse "fragment" propagating within a two-dimensional ring structure acquires a nonuniform curvature, so as to satisfy the no-flux boundary conditions applied on both curved boundaries (and the linear speed distribution required for it to propagate coherently). This can lead to a locally concave shape of the pulse (larger local velocity) close to the outer boundary and a locally convex shape (smaller local velocity) close to the inner boundary. The difference in the local curvature of the 2D pulse close to the inert boundaries contributes to the spatial structure of the unstable eigenmodes near the Hopf bifurcation point. We now study how the pulse responds to changes in r_i while keeping r_o fixed. In this case, as we vary r_i, both the curvature of the inner boundary and the distance between the two boundaries change. A typical bifurcation diagram with respect to r_i with fixed r_o is plotted in Fig. 6.

When r_i approaches the outer ring radius r_o, the pulse becomes effectively one-dimensional and propagates at a limiting velocity of approximately 0.6 s^{-1} (0.02 s^{-1} for ω with $r_o=30$), consistent with the value read from the one-dimensional pulse bifurcation diagram in Fig. 1. The qualitative structure of the bifurcation diagram in Fig. 6 is similar to that in Fig. 4.

The continuation of pulse solutions with respect to r_i for several fixed values of r_o is shown in Fig. 7. We see that, at criticality, the pulse speed at the inner boundary (the slowest linear speed along the pulse) does depend on the actual value of r_o (and thus the overall pulse shape and its nonuniform curvature). All three stable branches for different r_o converge to a distinct point at $r_i/r_o=1$, which corresponds to the one-dimensional problem (and so do, separately, all three unstable ones).

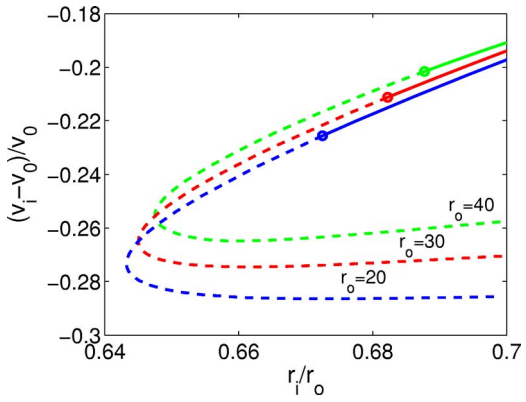

FIG. 7. (Color online) Bifurcation diagram varying the inner ring radius r_i while fixing r_o. The Hopf bifurcations are marked by circles. Solid (dashed) lines denote stable (unstable) steady pulse solutions. v_i is the local velocity of the propagating pulse at the inner boundary. v_0 is the propagating speed of a one-dimensional pulse. The v_i associated with the Hopf bifurcation point depends on r_o.

When the diffusion coefficient is sufficient small, the medium can no longer support a pulse solution; this is associated with a turning point on the continuation curve with respect to the diffusion coefficient at fixed r_i and r_o (not shown). Scaling both ring radii by a factor of k is equivalent to fixing the geometry but solving a problem with a diffusion coefficient scaled by a factor of $1/k^2$. This can be used to rationalize the movement of the bifurcation curves toward the right in Fig. 7: Using increasingly larger r_o should lead to a critical r_o above which there exists no pulse solution for a given r_i/r_o.

IV. DYNAMIC SIMULATIONS AND EXPERIMENTS

We now consider how the boundary-curvature-associated pulse instabilities manifest themselves in time for both simulations and experiments. A dynamic simulation close to (but just beyond) the Hopf bifurcation point shows an initial "tornadolike" oscillation of the "tip" of the pulse close to the inner boundary. This tip becomes increasingly thinner (as indicated by the color contours) and after some time the pulse "decollates" from the inner boundary and eventually dies out [Fig. 8(a)]. This transient eventually evolves to the spatially uniform steady state which is stable; thus the simulation is consistent with a subcritical Hopf bifurcation. The limit cycle branch is created unstable and "backward" in parameter space; the saddle-type limit cycle and its stable manifold constitute the separatrix between the stable pulse and the stable uniform solution when these coexist.

Figures 8(b) and 8(c) show this decollation mechanism from experimental observations of a CO-rich pulse in a sequence of still shots 0.28 s apart. The direction of motion of the pulse in the ring is denoted by an arrow. The data come from photoemission electron microscopy observations of CO oxidation on microdesigned Pt catalysts; the black areas are 2000 Å tall Ti layers, deposited through microlithography on the Pt(110) single crystal. The inner and outer rings of the

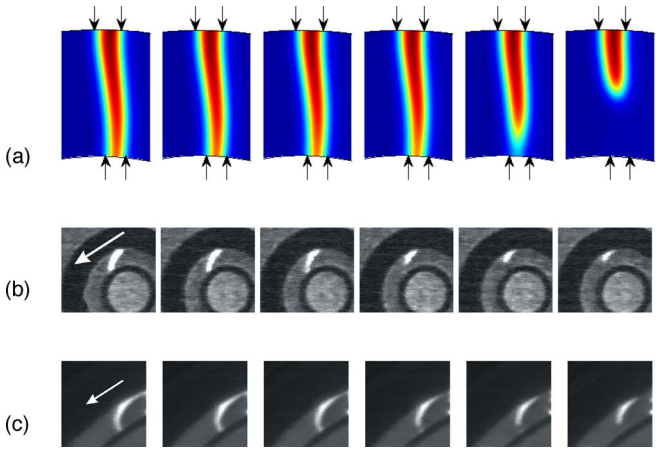

FIG. 8. (Color online) Sequences of snapshots showing the decollation of propagating pulses from the inner boundary of a ring structure. (a) Numerical simulation. The time interval between each snapshot is 2 s. Position-fixed arrows are used to show the change of the decollating pulse. The arrows are aligned to the boundary of the pulse in the first snapshot. The tip of the pulse at the inner boundary first slowly moves toward the left and shrinks at the same time; then it decollates from the boundary. (b) and (c) are experimental observations. The dark area is TiO_2 and the gray area is Pt(110). The white propagating pulse is a CO-rich one. Experimental conditions: T=447 K, $P_{O_2}=4\times10^{-4}$ mbar; $P_{CO}=$ (b) 3.35×10^{-5} and (c) 2.95×10^{-5} mbar.

ring-shaped Pt "corridor" between the tall Ti "walls" are 12.5 (160) and 20 (180) μm respectively in Fig. 8(b) [Fig. 8(c)]. The experimental conditions are given in the figure caption; one must remember, however, when observing these experiments that diffusion on the Pt(110) crystal is *anisotropic*. The thinning and decollation of the pulse close to the inner boundary can be clearly seen.

V. SUMMARY AND CONCLUSIONS

We studied the effect of operating conditions and of geometry (in particular, of boundary curvature) on the speed and stability of pulses in excitable media; our illustrative model described CO oxidation under high-vacuum conditions on Pt(110). The main instability is a decollation that occurs at the inner ring boundary; while the turning point bounding one-dimensional pulses still exists in full two-dimensional studies, the primary destabilization occurs earlier, before the turning point itself. We found that this primary instability involves a (subcritical) Hopf bifurcation, leading to the decollation of the pulse from the inner boundary, and (here) its eventual destruction.

In microdesigned on microstructured media, pulses often encounter sudden changes in curvature (for example, at corners or channel exits); a ring geometry—more precisely, a family of ring geometries with varying radii—allows for the systematic study of the effect of *steady*, controlled curvature. This provides insight into the basic boundary decollation instability which underpins many of the events occurring in more complex media. Dynamic pattern formation in microchannels is studied in many contexts beyond catalytic reactions (see, e.g., recent work in homogeneous reactions [37], and beyond reacting systems in microfluidics [38,39]). Boundary curvature and its variations is, we believe, a crucial factor in all such applications. Additional issues like boundary roughness (statistics of curvature at a much finer scale) as well as the use of *active* boundaries (e.g., consisting of a different catalyst; see Ref. [40]) will modify the results we described here. We believe, however, that the basic reacting front decollation from a curved boundary will be a recurring theme in all these contexts, and an important component of pattern formation in complex heterogeneous media.

ACKNOWLEDGMENTS

This work was partially supported by an NSF/ITR grant and by AFOSR (I.G.K., L.Q.); L.Q. gratefully acknowledges the support of the US DOE through PPPL.

[1] M. C. Cross and P. C. Hohenberg, Rev. Mod. Phys. **65**, 851 (1993).
[2] R. Imbihl, Catal. Today **105**, 206 (2005).
[3] H. H. Rotermund, W. Engel, M. Kordesch, and G. Ertl, Nature (London) **343**, 355 (1990).
[4] X. Jiang, D. A. Bruzewicz, A. P. Wong, M. Piel, and G. M. Whitesides, Proc. Natl. Acad. Sci. U.S.A. **102**, 975 (2004).
[5] M. Park, C. Harrison, P. M. Chaikin, R. A. Register, and D. H. Adamson, Science **276**, 1401 (1997).
[6] R. Verberg, C. M. Pooley, J. M. Yeomans, and A. C. Balazs, Phys. Rev. Lett. **93**, 184501 (2004).
[7] M. Böltau, S. Walheim, J. Mlynek, G. Krausch, and U. Steiner, Nature (London) **391**, 877 (1998).
[8] O. Steinbock, P. Kettunen, and K. Showalter, Science **269**, 1857 (1995).
[9] M. D. Graham, I. G. Kevrekidis, K. Asakura, J. Lauterbach, K. Krischer, H. H. Rotermund, and G. Ertl, Science **264**, 80 (1994).
[10] K. H. W. J. T. Tusscher and A. V. Panfilov, Multiscale Model. Simul. **3**, 265 (2005).
[11] G. Bub, A. Shrier, and L. Glass, Phys. Rev. Lett. **94**, 028105 (2005).
[12] A. Kaminaga, V. K. Vanag, and I. R. Epstein, Phys. Rev. Lett. **95**, 058302 (2005).
[13] H. A. Stone, A. D. Stroock, and A. Ajdari, Annu. Rev. Fluid Mech. **36**, 381 (2004).
[14] M. Joanicot and A. Ajdari, Science **309**, 887 (2005).
[15] A. D. Stroock, S. K. W. Dertinger, A. Ajdari, I. Mezić, H. A. Stone, and G. M. Whitesides, Science **295**, 647 (2002).
[16] J. Wolff, A. G. Papthanasiou, I. G. Kevrekidis, H. H. Rotermund, and G. Ertl, Science **294**, 134 (2001).
[17] T. Sakurai, E. Mihaliuk, F. Chirila, and K. Showalter, Science

296, 2009 (2002).
[18] E. M. Lucchetta, J. H. Lee, L. A. Fu, N. H. Patel, and R. F. Ismagilov, Nature (London) **434**, 1134 (2005).
[19] K. Agladze, J. P. Keener, S. C. Muller, and A. Panfilov, Science **264**, 1746 (1994).
[20] N. Hartmann, M. Bär, I. G. Kevrekidis, K. Krischer, and R. Imbihl, Phys. Rev. Lett. **76**, 1384 (1996).
[21] M. Bär, A. K. Bangia, I. G. Kevrekidis, G. Haas, H. H. Rotermund, and G. Ertl, J. Phys. Chem. **100**, 19106 (1996).
[22] C. Cabo, A. M. Pertsov, J. M. Davidenko, J. Jalife, Chaos **8**(1), 116 (1998).
[23] J. J. Tyson and J. P. Keener, Physica D **32**, 327 (1988).
[24] A. S. Mikhailov, *Foundations of Synergetics I: Distributed Active Systems* (Springer, New York, 1994).
[25] J. Krishnan, I. G. Kevrekidis, M. Or-Guil, M. G. Zimmerman, and M. Bär, Comput. Methods Appl. Mech. Eng. **170**, 253 (1999).
[26] M. Or-Guil, J. Krishnan, I. G. Kevrekidis, and M. Bär, Phys. Rev. E **64**, 046212 (2001).
[27] J. Krishnan, K. Engelborghs, M. Bär, K. Lust, D. Roose, and I. G. Kevrekidis, Physica D **154**, 85 (2001).
[28] M. Bär, N. Gottschalk, M. Eiswirth, and G. Ertl, J. Chem. Phys. **100**, 1202 (1994).
[29] K. Krischer, M. Eiswirth, and G. Ertl, J. Chem. Phys. **96**, 9161 (1992).
[30] E. G. Seebauer, A. C. F. Kong, and L. D. Schmidt, J. Chem. Phys. **88**, 6597 (1988).
[31] A commercial software package that is available at http://www.comsol.com
[32] C. T. Kelley, *Iterative Methods for Linear and Nonlinear Equations*, Frontiers in Applied Mathematics, Vol. 16 (SIAM, Philadelphia, 1995).
[33] C. W. Rowley and J. E. Marsden, Physica D **142**, 1 (2000).
[34] C. W. Rowley, I. G. Kevrekidis, J. E. Marsden, and K. Lust, Nonlinearity **16**, 1257 (2003).
[35] W. J. Beyn and V. Thümmler, SIAM J. Appl. Dyn. Syst. **3**, 85 (2004).
[36] M. Falcke, M. Bär, H. Engel, and M. Eiswirth, J. Chem. Phys. **97**, 4555 (1992).
[37] H. Kitahata, A. Yamada, S. Nakata, and T. Ichino, J. Phys. Chem. A **109**, 4973 (2005).
[38] O. Kuksenok, D. Jasnow, J. Yeomans, and A. C. Balazs, Phys. Rev. Lett. **91**, 108303 (2003).
[39] R. Dreyfus, P. Tabeling, and H. Willaime, Phys. Rev. Lett. **90**, 144505 (2003).
[40] X. Li, I. G. Kevrekidis, M. Pollmann, A. G. Papathanasiou, and H. H. Rotermund, Chaos **12**, 190 (2002).